Materials Letters 387 (2025) 138280

Contents lists available at ScienceDirect

Materials Letters

journal homepage: www.elsevier.com/locate/matlet

Effect of Ti on microstructure and mechanical properties of high strength AA6xxx alloy

P. Shurkin [a,*], G. Scamans [a,b], T. Subroto [c], N. Barekar [c], F. Sadeghi [a], J.L. Nebreda [a], C. Barbatti [c]

[a] BCAST, Brunel University of London, Uxbridge, Middlesex UB8 3PH, UK
[b] Innoval Technology, OX16 1TQ Banbury, Oxfordshire, UK
[c] Constellium UTC, Brunel University of London, UB8 3PH Uxbridge, Middlesex, UK

ARTICLE INFO

Keywords:
AA6xxx alloys
Ti
Zr
Intermetallics
Nanoindentation
Extrusion
Bending

ABSTRACT

Titanium is common in recycled aluminium alloys but limited in high-strength variants containing Zr and Cr. This study shows that Ti increases the liquidus temperature and promotes the formation of Al_3Ti-$(Al,Si)_3(Ti,Zr)$ core–shell intermetallics. Zr and Si absorption reduces hardness and enhances the plasticity of Al_3Ti intermetallic. Ti addition improved extruded profile bending performance due to a reduced peripheral coarse grain depth, while cracks propagated via voids at Fe-intermetallics rather than Ti-intermetallics.

1. Introduction

Most studies about recycled alloys focus on iron (Fe), but titanium impurity (Ti) is even more restricted. It has been established that Ti may accumulate with beverage cans recycling cycles due to TiO_2 particles in the decoration lacquer [1]. Furthermore, Ti is added upon every casting loop as an Al-Ti-B grain refiner with varying rates depending on the alloy. Cast Al-Si alloys, which are widely found in scrap [2], require 10 times more Al-Ti-B grain refiner compared to wrought alloys [3]. For alloys containing Zr and Cr, the addition of Al-Ti-B can be up to 3 kg/t compared to ~ 0.75 kg/t for conventional alloys [4]. Thus, Ti content may increase upon recycling.

Ti addition in Al alloys causes little solution hardening and no precipitation hardening [5]. The maximum Ti content to avoid primary Al_3Ti intermetallics is 0.12 wt.%Ti, the peritectic point in the binary Al-Ti phase diagram. Ti liquid solubility decreases in the presence of other elements, such as in liquid Al-Si alloy, forming TiAlSi intermetallics [6]. These blocky particles reduce ductility and cause casting feeding blockage. Recently, primary $(Al,Si)_3(Ti,Zr)$-$D0_{22}/D0_{23}$ intermetallics were produced and characterized, showing Ti does not stabilize these intermetallics compared to Si [7]. For AA6082 with 0.2 %Zr and 0.1 %Ti additions, the Al-Zr-Ti-Si intermetallics were refined by ultrasonic treatment to improve grain refining [8]. However, their formation mechanisms, properties, and bulk effects remain unreported.

In this letter, we discuss the effect of excess Ti addition on the formation of primary intermetallics and mechanical properties of Zr-containing AA6xxx industrial-scale billet and extrusion products.

2. Materials and methods

AA6111-type aluminium alloy containing Ti + Zr < 0.25 wt% was the object of this study. Ti content was 0.04 wt% for the reference alloy and 0.1 wt% for the Ti-excess alloy. Al-10wt.%Ti master alloy was added for excess Ti. The alloy was grain refined using 3 kg/t Al-3Ti-1B and a direct-chill casting was used to produce 152 mm diameter billets [9]. Commercial homogenization was followed by extrusion on a 1600 t extrusion press into a flat profile with an extrusion ratio of 72. After press-quenching, the solutionised components were aged for maximum strength (T6). Identical casting and processing parameters were provided for both alloys. Microstructure was studied using an optical microscope (OM) Zeiss Axio Scope A1, and a scanning electron microscope (SEM) Zeiss Gemini Supra 55 VP at 20 kV in backscattered electron mode (BSE), and energy-dispersive spectroscopy (EDS). Etching in 10 vol% HCl aqueous solution was used to reveal the three-dimensional morphology of intermetallics. Pandat software with the PanAl2021 database was used for thermodynamic calculations. Nanoindentation

* Corresponding author.
E-mail address: pavel.shurkin@brunel.ac.uk (P. Shurkin).

https://doi.org/10.1016/j.matlet.2025.138280
Received 17 February 2025; Accepted 21 February 2025
Available online 22 February 2025

was conducted at a 20 mN peak load using a calibrated NanoTest system with a Berkovich diamond indenter. A VDA 238–100 three-point bending test of extruded samples was conducted with bending axis perpendicular to the extrusion direction. The corrected bending angle (α') was calculated using the formula $\alpha' = \alpha \times \sqrt{h'/h}$, where α corresponds to a bending angle, h' is a sample thickness and h is a reference sample thickness (taken as 2.0 mm).

3. Results and discussion

Both reference and Ti-excess alloys had a mean grain size of 100 μm accounting for the excessive addition of Al-Ti-B. Fig. 1a shows primary particles in the grain interior indicating heterogeneous nucleation of (Al) grains, efficient for Zr and Ti-containing trialuminides [7,10]. Fig. 1b reveals that the primary intermetallics (IMCs) have a core–shell structure showing a complete wetting took place [11]. The phase diagram (Fig. 1c) shows the association of the observed particles with Ti and Zr. The Al_3Ti and Al_3Zr phases, peritectically transforming into (Al), dominate in the given temperature range. Ti-excess alloy with 0.1 wt.% Ti has a liquidus temperature of 730 °C, 60 °C higher than the reference alloy with 0.04 wt.%Ti, explaining the limitation of Ti in AA6xxx alloys.

Different composition of the core and shell IMCs is evidenced by SEM/BSE (Fig. 2a) and EDS mapping (Fig. 2b) revealing Zr and Si segregation in the shell. EDS results (Table 1) indicate that the core phase corresponds to the Al_3Ti, while the stoichiometry of the shell phase reveals a $(Al_{1-x}Si_x)_3(Ti_{1-y}Zr_y)$ compound, referred to as $(Al,Si)_3(Ti,Zr)$. Deep etching revealed that the primary IMCs have a plate-like morphology with a thickness < 10 μm (Fig. 2c). The particle shown in Fig. 2a is likely a 2D cross-section of the three-dimensional plate which has a 2-μm thick Zr- and Si-rich envelope and several compositionally similar octahedral particles.

The observed phenomena may parallel Zr and Si poisoning of Al-Ti-B-based grain refiners due to lower free energy of Al_3Zr formation compared to Al_3Ti in the case of Zr [12] and strong Ti-Si covalent bond in the case of Si [13], thus leading to a dissolution of the two-dimensional Al_3Ti compound on the TiB_2 particle. While the latter was observed at the nanoscale, the current study observed the results of the interaction of Zr- and Si-rich melt with primary Al_3Ti even under optical microscopy.

Whereas the phase diagram predicts the formation of Al_3Ti and Al_3Zr phases (Fig. 1c), the suggested mechanism involves the segregation of Zr and Si at the Al_3Ti interface, followed by the diffusion-driven formation of the $(Al,Si)_3(Ti,Zr)$. Such phase formation is time-dependent assuming that enough diffusion time leads to the complete disappearance of the Al_3Ti phase. For instance, relatively small individual $(Al,Si)_3(Ti,Zr)$ particles are visible in Fig. 2a. Similarly, in [14], Al_3Ti particles surrounded by a TiAlSi envelope disappear after prolonged holding.

Typical nanoindentation load–displacement curves (Fig. 2d) show the differences in hardness from the varying peak depths. Whereas both IMCs exhibit a larger hardness and modulus compared to the (Al) matrix, the $(Al,Si)_3(Ti,Zr)$ has a ~ 40 % lower hardness and ~ 18 % lower elastic modulus (Table 1). However, compared to the literature hardness of dominating $Al_{15}(Fe,Mn)_3Si_2$ intermetallic (Fe-IMCs), ~10 GPa [15], the observed $(Al,Si)_3(Ti, Zr)$ phase is softer which may help alleviate the stress concentration and delay crack initiation upon strain.

Whereas Fe-IMCs fractured during the extrusion of Reference (Fig. 3a) and Ti-excess alloy (Fig. 3b), the core–shell particles retained their morphology likely owing to their improved plasticity. Considering the composition of the $(Al,Si)_3(Ti,Zr)$ IMC and their estimated fraction of ~ 0.035 %, the estimated reduction of solute Zr is 0.007 wt% and that of solute Si is 0.002 wt% which is negligible. This explains no deterioration of mechanical properties due to Ti as evidenced in the bending force–displacement curve normalized by the distance between rollers (L_0), thickness (t) and width of the sample (w) (Fig. 3c). The Ti-excess alloy performed 20 % improved bending than the reference alloy despite the primary particles. This improvement is attributed to a decreased thickness of the peripheral coarse grains (PCG) and good plasticity of $(Al,Si)_3(Ti,Zr)$ [16]. The PCG layer in the reference alloy (Fig. 3d) initiated the cracking at the outer surface initiating the reduction in wall thickness and drop in bending force. In contrast, Ti-excess alloy (Fig. 3e) demonstrates a ~ 3 times reduction in PCG depth accounting for the harder crack propagation through the fibres and force drop at the later stage. Crack propagation is facilitated by void nucleation at Fe-IMCs rather than at Ti-IMCs.

4. Conclusions

Primary Al_3Ti-$(Al,Si)_3(Ti,Zr)$ core–shell particles formed by diffusion-guided transformation in DC cast AA6xxx alloy as a result of an increase in Ti content and liquidus temperature respectively. The $(Al,Si)_3(Ti,Zr)$ IMC has a 40 % reduced hardness compared to binary trialuminide and they both retain morphology after hot extrusion compared to fractured Fe-IMCs. Primary particles were not facing the crack tip during bending failure, and the bending performance was even improved for Ti-excess alloy owing to the smaller PCG depth.

CRediT authorship contribution statement

P. Shurkin: Conceptualization, Data curation, Formal analysis, Investigation, Methodology, Writing – original draft, Writing – review & editing. **G. Scamans:** Funding acquisition, Project administration, Resources. **T. Subroto:** Project administration, Resources. **N. Barekar:** Resources, Supervision. **F. Sadeghi:** Validation, Writing – review & editing. **J.L. Nebreda:** Methodology, Writing – review & editing. **C. Barbatti:** Project administration, Resources, Supervision, Writing – review & editing.

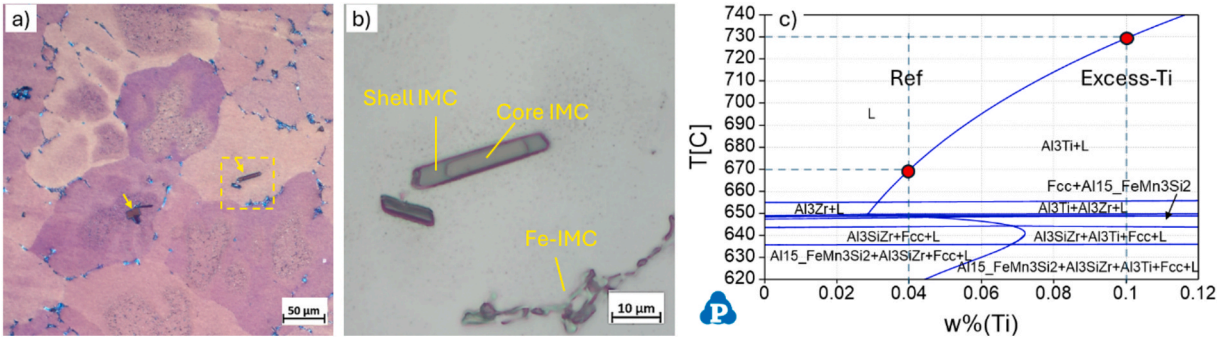

Fig. 1. Micrograph of primary IMCs in the Ti-excess alloy obtained using polarized light in OM (a); magnified view of core–shell primary IMCs (b); and vertical isopleth showing the influence of Ti on equilibrium phase composition (c).

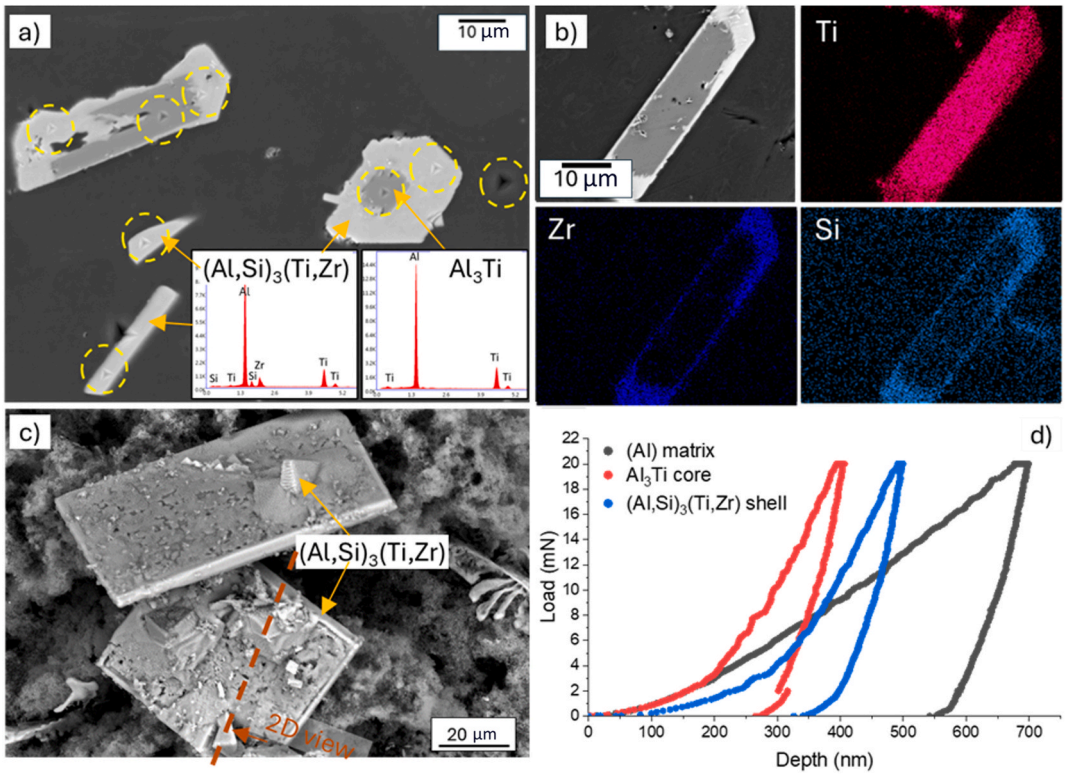

Fig. 2. SEM/BSE image of the Al_3Ti-$(Al,Si)_3(Ti,Zr)$ IMCs with arrowed nanoindentation marks (a); EDS mapping (b); microstructure after deep etching (c); nanoindentation load–displacement curves (d).

Table 1
EDS (at.%) and nanoindentation results for Ti-excess alloy.

Phase	Al	Si	Ti	Zr	Fe	Mn	Hardness, GPa	Elastic modulus, GPa
(Al) matrix	Balance	0.7	0	0	0	0.2	1.9 ± 0.6	70.9 ± 4.2
Al_3Ti core	Balance	0	24.4	0	0	0	6.5 ± 0.7	163.3 ± 6.1
$(Al,Si)_3(Ti,Zr)$ shell	Balance	4.6	16	7.2	0	0	4.0 ± 0.3	134.2 ± 4.9

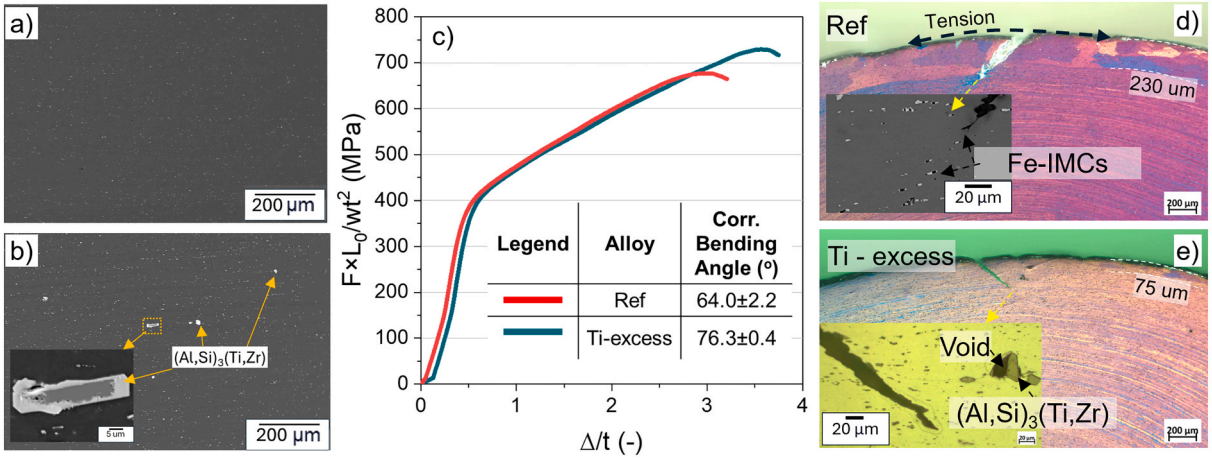

Fig. 3. SEM/BSE micrographs of extruded Reference (a) and Ti-excess alloy (b); Force vs. Displacement curve recorded during VDA 238–100 bending test (c); crack observation under cross-polarized light in Reference (d) and Ti-excess alloy (e).

Declaration of competing interest

The authors declare the following financial interests/personal relationships which may be considered as potential competing interests: Pavel Shurkin reports financial support, administrative support, and article publishing charges were provided by Brunel University London. The authors declare that they have no known competing financial interests or personal relationships that could have appeared to influence the work reported in this paper. If there are other authors, they declare that they have no known competing financial interests or personal

relationships that could have appeared to influence the work reported in this paper.

Acknowledgements

The authors gratefully acknowledge the grant to Brunel University received from the Advanced Propulsion Centre through Innovate UK that supported the work programme presented.

Data availability

Data will be made available on request.

References

[1] A.N. Løvik, D.B. Müller, A Material Flow Model for Impurity Accμmulation in Beverage Can Recycling Systems, in: J. Grandfield (Ed.), Light Metals 2014, 1st ed., Wiley, 2014: pp. 907–911. https://doi.org/10.1002/9781118888438.ch151.

[2] R.G. Billy, D.B. Müller, Aluminiμm use in passenger cars poses systemic challenges for recycling and GHG emissions, Resour. Conserv. Recycl. 190 (2023) 106827, https://doi.org/10.1016/j.resconrec.2022.106827.

[3] Y. Birol, AlB3 master alloy to grain refine AlSi10Mg and AlSi12Cu aluminiμm foundry alloys, J. Alloy. Compd. 513 (2012) 150–153, https://doi.org/10.1016/j.jallcom.2011.10.010.

[4] R. Vainik, Managing Grain Refining Efficiency: The Way Forward for Aluminμm Casthouses, LMA 78 (2020) 56–61.

[5] K.E. Knipling, D.C. Dunand, D.N. Seidman, Nucleation and Precipitation Strengthening in Dilute Al-Ti and Al-Zr Alloys, Metall. Mater. Trans. A 38 (2007) 2552–2563, https://doi.org/10.1007/s11661-007-9283-6.

[6] X.-G. Chen, M. Fortier, TiAlSi intermetallic formation and its impact on the casting processing in Al–Si alloys, J. Mater. Process. Technol. 210 (2010) 1780–1786, https://doi.org/10.1016/j.jmatprotec.2010.06.009.

[7] J.-R. Castillo-Sánchez, G. Salloμm-Abou-Jaoude, A.E. Gheribi, P. Lafaye, K. Oishi, J.-P. Masse, E. Bousser, G. L'Espérance, J.-P. Harvey, Synthesis and characterization of $(Al,Si)_3(Zr,Ti)$-$D0_{22}/D0_{23}$ intermetallics: Understanding the stability of silicon substitution, Acta Mater. 262 (2024) 119455, https://doi.org/10.1016/j.actamat.2023.119455.

[8] G. Salloμm-Abou-Jaoude, D.G. Eskin, C. Barbatti, P. Jarry, M. Jarrett, Z. Fan, Effect of Ultrasonic Processing on a Direct Chill Cast AA6082 Aluminiμm Alloy, in: A. P. Ratvik (Ed.), Light Metals 2017, Springer International Publishing, Cham, 2017, pp. 997–1003, https://doi.org/10.1007/978-3-319-51541-0_120.

[9] N.S. Barekar, I. Skalicky, S. Wang, P. Shurkin, O. Adole, N.H. Babu, M. Jarrett, Comparative Analysis of Structure and Properties of Nb-B Inoculated Direct Chill Cast AA4032 Alloy Extruded from As-Cast and Homogenized Conditions, JOM 74 (2022) 1218–1227, https://doi.org/10.1007/s11837-021-05134-7.

[10] Z. Chen, K. Yan, Grain refinement of commercially pure aluminμm with addition of Ti and Zr elements based on crystallography orientation, Sci. Rep. 10 (2020) 16591, https://doi.org/10.1038/s41598-020-73799-2.

[11] B.B.Straumal, A.Korneva , G.A.Lopez , A.Kuzmin, E.Rabkin , G.Gerstein, A. Straumal, A.S.Gornakova AS. Grain Boundary Wetting by a Second Solid Phase in the High Entropy Alloys: A Review. Materials. 14 (2021); 7506. https://doi.org/10.3390/ma14247506.

[12] Y. Wang, C.M. Fang, L. Zhou, T. Hashimoto, X. Zhou, Q.M. Ramasse, Z. Fan, Mechanism for Zr poisoning of Al-Ti-B based grain refiners, Acta Mater. 164 (2019) 428–439, https://doi.org/10.1016/j.actamat.2018.10.056.

[13] Y. Wang, Z. Que, T. Hashimoto, X. Zhou, Z. Fan, Mechanism for Si Poisoning of Al-Ti-B Grain Refiners in Al Alloys, Metall. Mater. Trans. A 51 (2020) 5743–5757, https://doi.org/10.1007/s11661-020-05950-7.

[14] T. Gao, G. Liu, X. Liu, Compositions and morphologies of TiAlSi intermetallics in different diffusion couples, Mater Charact 95 (2014) 285–290, https://doi.org/10.1016/j.matchar.2014.07.009.

[15] C.-L. Chen, A. Richter, R.C. Thomson, Mechanical properties of intermetallic phases in multi-component Al–Si alloys using nanoindentation, Intermetallics 17 (2009) 634–641, https://doi.org/10.1016/j.intermet.2009.02.003.

[16] M.V. Karpets, Y.V. Milman, O.M. Barabash, N.P. Korzhova, O.N. Senkov, D. B. Miracle, T.N. Legkaya, I.V. Voskoboynik, The influence of Zr alloying on the structure and properties of Al3Ti, Intermetallics 11 (2003) 241–249, https://doi.org/10.1016/S0966-9795(02)00234-0.